JOURNAL OF MATERIALS SCIENCE 30 (1995) 5356–5370

The effects of ion implantation on the friction behaviour of sapphire

S. J. BULL
AEA Technology, Building 552, Harwell Laboratory, Didcot, Oxfordshire OX11 ORA, UK
T. F. PAGE
Department of Metallurgy and Engineering Materials, The University, Newcastle-upon-Tyne NE1 7RU, UK

The friction behaviour of ion-implanted sapphire in contact with diamond cones and spheres of a range of materials has been investigated as a function of implantation dose and implant species. Generally, an increase in friction is observed at low doses followed by a decrease once amorphization takes place. For the sharp diamond cones this can be correlated with changes in ploughing behaviour controlled by near-surface plasticity, whereas, for the spheres, the increase in friction for low-dose implants is due to changes in adhesion between the spheres and the implanted layer. The implications of these observations for the creation of lubricating surface layers by high-dose ion implantation are discussed.

1. Introduction

The friction and wear properties of ceramic (and other) materials are primarily a function of the mechanical, physical and chemical properties of the contacting surfaces (e.g. [1–4]). Ion implantation is a technique which can change the composition, microstructure and properties in the surface and near-surface region and should thus have important effects on tribology, particularly in cases where any depth of material removal or damage by wear is small compared to the thickness of the implanted layer. Indeed, ion implantation into metals has been shown to increase hardness and decrease both friction and wear in some cases [5, 6]. For ceramics, however, amorphization, the enforced creation of unusual solid solutions or even the formation of new phases can result from ion implantation (with or without post-implantation heat treatment) [7–14]: in turn, these microstructural modifications are expected to effect changes in the mechanism of surface deformation and thus variously modify the material's responses, controlling friction and different types of wear.

The majority of wear studies for ion-implanted ceramics have been performed using the single-pass scratch test (e.g. [7, 9, 15, 16]). Thus, in implanted materials, the presence of surface compressive stresses has been shown to result in a reduction in the amount of radial and lateral fracture around the scratch. Thus the amount of brittle abrasive wear, together with concomitant energy absorption and hence friction, is reduced. At low doses, where surface hardening occurs, the width of the scratch track is observed to be reduced as the amount of plastic abrasive wear is reduced. After the onset of amorphization, plastic deformation in the amorphous layer dominates the wear behaviour, because even after some stress relief has occurred, the surface compressive stresses are large enough to reduce drastically the amount of surface fracture compared to unimplanted material [17]. Changes in friction for metals produced by ion implantation have been reported following pin-on-disc studies [18, 19]. In general, friction was found to be reduced after implantation. Similar studies for ceramics were initially inconclusive [20], but later results showed that, for sapphire, the friction increases after low-dose implantation [21]. In addition to changes in friction due to changes in the mechanical properties of implanted surfaces, it has been shown that the contribution to friction from adhesion between the sliding surfaces can be changed by ion implantation [22]. For magnesium oxide substrates, the friction against diamond slider cones with hemispherical tips was observed to increase dramatically after low-dose titanium implantation. This was associated with the desorption of surface adsorbates during the implantation process and a reduced propensity for reforming the adsorbate layers on subsequent exposure to the atmosphere. The effect is dramatic for MgO, but much less pronounced in the case of the sapphire substrates investigated in this study.

In this study, we have used the single-pass scratch test to investigate the changes to the measured friction produced by implantation over a wide dose range. The frictional changes are analysed in terms of their components and conclusions drawn about using ion implantation for improving the tribological behaviour of ceramics. For the first time, it has been possible to separate the adhesion and ploughing contributions to friction and estimate the changes to these effects by implantation.

0022–2461

TABLE I Range and damage parameters for the materials implanted in this study

Target	Ion	Ion energy, E_0 (keV)	Projected mean ion range, R_p (μm)	Standard deviation, ΔR_p (μm)	Projected mean damage depth, X_d (μm)	Standard deviation, ΔX_d (μm)	Energy loss in displacement damage processes, E_c (keV ion^{-1})
Sapphire	Ti	300	0.143	0.041	0.088	0.051	125
Sapphire	Y	300	0.031	0.023	0.046	0.028	152

2. Experimental procedure

Single-crystal sapphire wafers of $(1\,0\,\bar{1}\,2)$ orientation (supplied by GEC, Wembley, UK), and prepolished to a device-level surface finish $R_a = 20$ nm, were cleaved into 20 mm × 20 mm × 0.1 mm sections, carefully degreased in alcohol and ultrasonically cleaned prior to implantation. The samples were then implanted with yttrium and titanium ions in the Cockcroft-Walton facility at UKAEA Harwell to doses in the range 10^{16} to 5×10^{17} ions cm^{-2}. All implantations were performed at room temperature with a beam current of a few microamps so that beam heating was estimated to be 250 °C at most. Implantation conditions and the range and damage parameters of the implanted ions are summarized in Table I.

Friction measurements were performed using a diamond stylus with a spherical tip attached to a single-pass scratch tester [17]. The tangential frictional force was measured with an instrumented arm and recorded on a chart recorder. This was averaged over the length of a track and divided by the load to determine the coefficient of friction. Passes were made parallel to $[\bar{1}\,0\,1\,0]$ at a speed of 0.25 m s^{-1} up to a maximum of 8 mm in length. The diamond styli were 90° cones with approximately spherical tips (supplied by Shaw Abrasives) which were initially found to have a number of angular asperities which were broken off or polished smooth in the first few scratches made at high loads (> 500 g). Thus the cones were worn in by repeated scratching of unimplanted sapphire at 500 g load until no further changes in the diamond profile could be detected by scanning electron microscopy (SEM). After this treatment the radii of curvature of the cones (perpendicular to the scratch direction) were determined from scanning electron micrographs and are given in Table II. The radii of curvature in other directions were found to be similar. Cones were only used for scratching or unimplanted layers after they had been run-in and no further profile changes were observed. The diamond sliders were investigated before and after scratching of the implanted materials but no change in diamond profile was observed. The cones were carefully degreased and ultrasonically cleaned, together with the flats, prior to scratch testing.

Further friction measurements were also performed with 3 mm sapphire spheres, steel (1%C, 1%Cr used in a hardened and tempered state (1000 VHN)) and WC/Co. These were cleaned and degreased using the same procedure as used for the scratch diamonds and scratches were made in the same crystallographic orientations. No running in was necessary.

TABLE II Radii of diamond cone tips

Substrate	Ion	Cone radius (μm)
Sapphire	Ti	148
Sapphire	Y	40

3. Analysis of friction results

According to the long-established theories of Bowden and Tabor [2], the measured friction will arise from a number of contributions.

1. *Adhesion.* When two surfaces are pressed in contact, junctions will be formed which are large compared to molecular dimensions. During sliding these junctions will be sheared and consequently may increase in size. For metals the shear strength of the adhesive bond determines the friction behaviour; in many cases the interfacial bond is stronger than the softer of the two materials and thus shear failure occurs within the soft material, resulting in transfer of material from the soft to the hard sliding face. For ceramics (where true junction welding may be difficult), failure is much more localized at or near the sliding interface so the shear strength of the contacting asperities will be important in determining the measured friction. The detailed origins of the forces of interfacial adhesion will be critically dependent on the surface condition (chemistry, topography, etc.) of the contacting materials and it is likely that ion implantation will also affect these.

The friction force will be determined by the true area of contact A_1, and the shear strength of the junction (or the softer material) τ, and is given by

$$F = A_1 \tau \quad (1)$$

For calculation purposes, the true area of contact A_1 must be measured which, in virtually all cases, is experimentally difficult. Thus estimates of the apparent area of contact are often used in these situations, based on the contact of perfectly smooth surfaces.

2. *Ploughing.* If one of the surfaces is harder than the other, then an asperity in the harder material may plough its way through the softer material resulting in the formation of a groove. The majority of the plastic deformation which occurs during the scratch test is

associated with groove formation and is included in this term. However, shearing of one or other of the sliding counterfaces may indeed result in plastic deformation which does not necessarily lead to groove formation. This is important in junction formation; the ploughing and adhesion terms are thus interrelated. According to Bowden and Tabor [2] the friction force due to ploughing is given by

$$F = A_2 P' \tag{2}$$

where A_2 is the projected cross-sectional area of the track and P' is the mean pressure to displace material in the surface. For an asperity modelled as a spherical cap

$$A_2 \approx d^3/12R \tag{3}$$

where d is the scratch track width and R the radius of the scratching particle. In general, ploughing friction is small compared to adhesion friction.

3. *Surface roughness.* The interaction between the asperities of two contacting surfaces can have a marked effect on the frictional force. Work must be done in deforming asperities of the softer material in order for one material to slide past another. Such deformation may be elastic or require some plasticity. For the plastic deformation of asperities, analysis by slip-line field theory shows that the effect on the frictional force is dependent on the average slope of the asperities [23]. However, for the materials investigated in this study, elastic deformation will be more important and an upper limit to the friction contribution from roughness in this case is given by

$$\mu = \tan\theta \tag{4}$$

where θ is the mean slope of the asperities. For most polished materials $\theta \leq 1°$ and thus $\mu \leq 0.017$ which is small compared to most measurements made and can thus be ignored.

4. *Fracture.* At high contact stresses significant amounts of cracking can occur around scratches in brittle materials. In this case, there are large oscillations in the friction trace along a scratch track and much of the frictional energy is dissipated in fracture processes. This has been modelled by Lawn and Swain [24] who obtained an expression for the friction coefficient in terms of the fracture toughness for scratches produced with a sharp indenter which is similar to the relationships obtained for static indentations derived by Lawn and co-workers [25–28]. In our study, loads were chosen so that no cracking occurred around the scratches in order to remove this effect from the calculations.

The total friction force may thus be expressed as the sum of these contributions

$$F = A_1\tau + A_2 P' \tag{5}$$

In practice, the components are not fully independent [28] but Equation 5 remains a reasonable approximation for the cases investigated here.

P' is a measure of surface plasticity which can be taken as the scratch hardness of the material given by

$$P' = kL/d^2 \tag{6}$$

where L is the applied load and k is a constant. Effectively A_1, the area of contact, is thus equal to d^2/k. Combining Equations 3, 5 and 6, we have

$$F = d^2\tau/k + kdL/12R \tag{7}$$

There are various ways of determining k but, if it is assumed that the load is supported on the front half of the moving stylus during sliding, then $k = 8/\pi$ which has been used in this study. Alternatively, $k = 2$ has been used [29], but this does not significantly alter the magnitude of the calculated ploughing friction.

From Equation 7 the interfacial shear strength, τ, can be calculated in terms of the measured friction force, F, the width of the scratch track, d, and the factors fixed by the experimental apparatus (tip radius, R, and applied load, L). However the use of Equation 7 relies on knowledge of the areas A_1 and A_2 and much better approximations are available from the work of Goddard and Willman [30] detailed elsewhere [4]. By this approach, the shear and ploughing forces on an element in the contact region are integrated over taken to be the front half of a hemispherical slider. The ploughing force is then given by

$$F = PR^2\left\{\sin^{-1}\left(\frac{d}{2R}\right) - \frac{d}{2R}\left[1 - \left(\frac{d}{2R}\right)^2\right]^{1/2}\right\} \tag{8}$$

and the adhesion component by

$$F = 2\tau R^2\left\{1 - \left[1 - \left(\frac{d}{2R}\right)^2\right]^{1/2}\right\} \tag{9}$$

If it is assumed that the applied load is also supported on the front half of the spherical slider, then

$$L = \pi d^2 P/8 \tag{10}$$

Dividing Equations 8 and 9 by Equation 10 gives the coefficient of friction due to ploughing, μ_p, and adhesion, μ_a, respectively

$$\mu_p = \left(\frac{2}{\pi}\right)\left(\frac{2R}{d}\right)^2\left\{\sin^{-1}\left(\frac{d}{2R}\right) - \left(\frac{d}{2R}\right) \times\left[1 - \left(\frac{d}{2R}\right)^2\right]^{1/2}\right\} \tag{11}$$

$$\mu_a = 2\left(\frac{2}{\pi}\right)\left(\frac{2R}{d}\right)^2\left(\frac{\tau}{P}\right)\left\{1 - \left[1 - \left(\frac{d}{2R}\right)^2\right]^{1/2}\right\} \tag{12}$$

From these expressions it can be seen that μ_p can be calculated from the measured track width and the radius of the stylus. However, μ_a depends on the ratio τ/P which needs to be determined.

If P is taken as the hardness of the material, then

$$P = cY \tag{13}$$

where c is a constant and Y the uniaxial yield stress. The value of c depends on the ratio of Young's modulus to yield stress which, for many materials it is close to 3, though for some ceramics can be very much less [31].

From the Tresca yield criterion [32] we have

$$\tau = Y/2 \tag{14}$$

where τ and Y are the shear yield and uniaxial tensile yield stresses, respectively. Combining Equations 13

and 14 gives

$$\frac{\tau}{P} = \frac{1}{2c} \tag{15}$$

which leads to a theoretical value for this ratio of one-sixth if the adhesion friction force is dominated by shearing of the ploughed material. Ceramics would be expected to have τ/P ratios less than 0.17 by this argument as the constant c in Equation 13 can be as low as 2.4. In this study values of τ/P have been calculated from experimental data using Equations 11 and 12 and the approximation

$$\mu_{measured} = \mu_a + \mu_p \tag{16}$$

The shear strength, τ, can then be calculated from the τ/P ratio using values of P determined from Equation 10. The low friction coefficient comes from the lack of true welding such that $\tau_{slide} \ll Y/2$.

4. Results and discussion

4.1. Single-pass friction traces: single-crystal sapphire

There are two friction coefficients which can be important for understanding wear behaviour, namely static friction which is a measure of the friction force which is recorded at the onset of relative motion of two sliding surfaces, and dynamic friction which is the steady state value once sliding motion is established. These are not usually the same for either unimplanted or implanted materials. The static friction value is dominated by adhesion and is more a function of surface cleanliness than dynamic friction. In general, it has been found that, for low-load scratch tests where little or no plastic deformation occurs, static friction exceeds dynamic friction, whereas at higher loads where a well-defined scratch track is produced, the dynamic friction is larger and can increase along the track length. In this section we present single-pass friction traces for sapphire implanted with yttrium and titanium which illustrate these effects.

Fig. 1 shows graphs of friction force against sliding distance for the scratches on titanium-implanted sapphire. The traces show a rapid increase in friction in the first ~ 0.5 mm of travel, leading to a more constant value which oscillates about a mean value at longer sliding distances. The sliding distance quoted here is merely the distance through which the specimen table has been driven. Thus it is most likely that the initial rapid increase corresponds to the deflection of the beam whilst the static friction increases. Once the stylus begins to move the friction tends to drop (though this does not happen in all cases and is by no means repeatable) indicating that the static friction is somewhat higher than the dynamic friction.

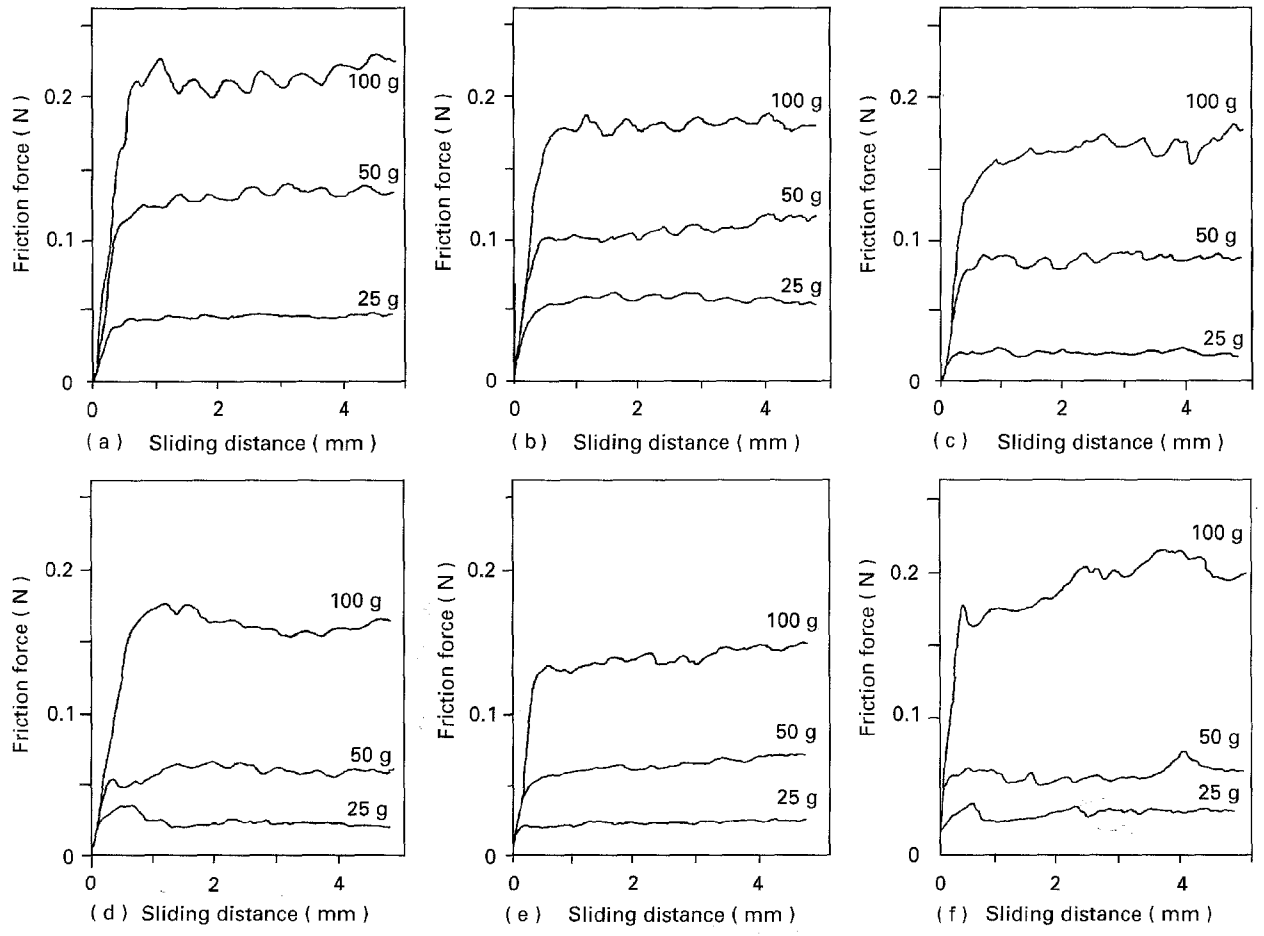

Figure 1 Typical experimental variation of the friction force with sliding distance for titanium-implanted $(10\bar{1}2)$ sapphire scratched with a diamond cone. The friction increases up to the value when relative motion between the cone and flat begins (the so-called "static" or "limiting" friction) and then levels off to oscillate about a mean value ("stick–slip"). This mean kinetic friction has been used throughout this study. (a) Unimplanted, (b) 10^{16} Ti^+ cm^{-2}, (c) 2×10^{16} Ti^+ cm^{-2}, (d) 5×10^{16} Ti^+ cm^{-2}, (e) 10^{17} Ti^+ cm^{-2}, (f) 5×10^{17} Ti^+ cm^{-2}.

The oscillations in the track once the stylus has begun to move are due to stick–slip motion. As the force of the stylus increases, the friction increases until the stylus begins to move; the friction force is then reduced and the arm starts to straighten, leaving a net restoring force on the stylus. The stylus then slides over the flat until it sticks, comes to rest again, and the process is repeated. Thus the observed response depends in part on the compliance of the tester arm. The ideal friction trace for this behaviour is a saw tooth, but the response of the machine to these rapid oscillations is too slow to record this and the resultant trace contains a number of regularly spaced humps. As the dose of titanium is increased the stick–slip oscillations become less pronounced. This is an indication that the adhesion between the diamond and the implanted surfaces has changed (see Section 4.3).

Fig. 2 shows similar traces for yttrium implanted sapphire. From the unimplanted friction traces it can be seen that the friction force gradually increases with sliding distance. This is presumed due to the build up of debris in front of the moving stylus as the measured widths of the scratch tracks do not change along their length once motion has started. Another feature of the friction traces in this material is that the highest dose specimens show a decrease in friction with sliding distance. These specimens all have soft amorphous layers and thus it could be that the debris produced by the stylus is acting as a lubricant. Fig. 3 shows scratches in unimplanted and 5×10^{17} Y ions cm^{-2} implanted sapphire. The debris produced from the unimplanted material is sharp and angular and thus has its origins in brittle fracture around the scratch. By contrast, the debris produced from the high-dose implanted material is more rounded indicating its origin in plastic deformation. This debris could act as a lubricant if it rolls between the stylus and the implanted surface.

In these materials scratches were made with loads up to 100 g at which load fracture around the scratches began to occur causing rapid oscillations in the friction trace. The lateral compressive stresses associated with ion implantation reduce this fracture so that, whereas cracking occurs around scratches in unimplanted material at 100 g loads, no similar cracks were observed for any of the implanted materials. For 100 g loads the widths of the scratch track produced for yttrium and titanium implants were measured as 7.75 and 11.25 μm, respectively, corresponding to penetration depths of 0.09 and 0.05 μm, respectively. Thus the scratches are expected to lie predominantly in the implanted layer (see Table I).

Coefficients of sliding friction, μ, were determined by taking the mean value of friction force averaged along the track and dividing by the normal load. In order to avoid the contribution due to fracture, only

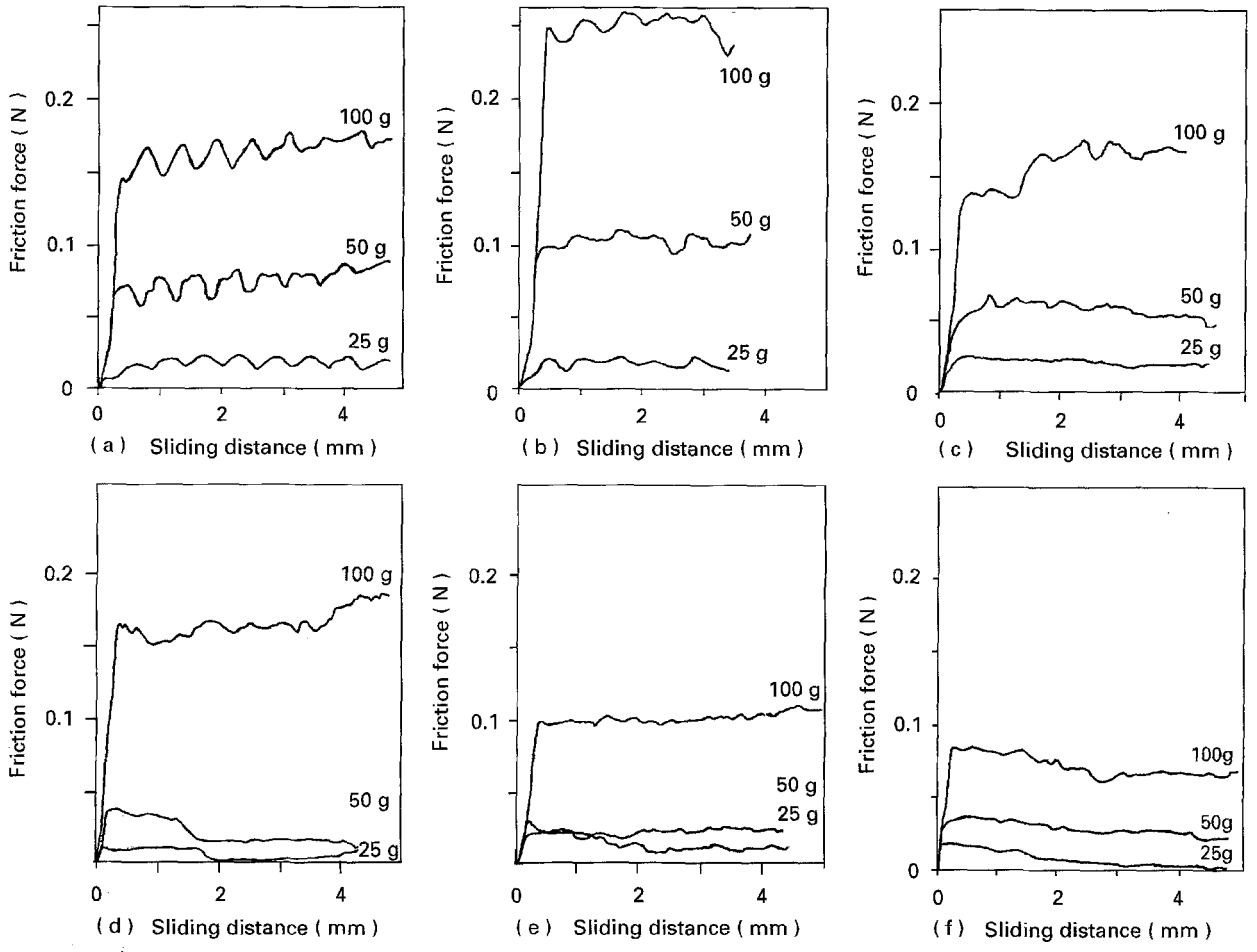

Figure 2 Typical experimental variation of the friction force with sliding distance for yttrium-implanted $(10\bar{1}2)$ sapphire. The friction increases initially and then oscillates about a mean value once sliding had started. These stick–slip oscillations tend to be less pronounced as the dose of implanted ion is increased. The friction coefficient initially increases at low doses, but is reduced at high doses. (a) Unimplanted, (b) 10^{16} Y^+ cm^{-2}, (c) 2×10^{16} Y^+ cm^{-2}, (d) 5×10^{16} Y^+ cm^{-2}, (e) 10^{17} Y^+ cm^{-2}, (f) 5×10^{17} Y^+ cm^{-2}.

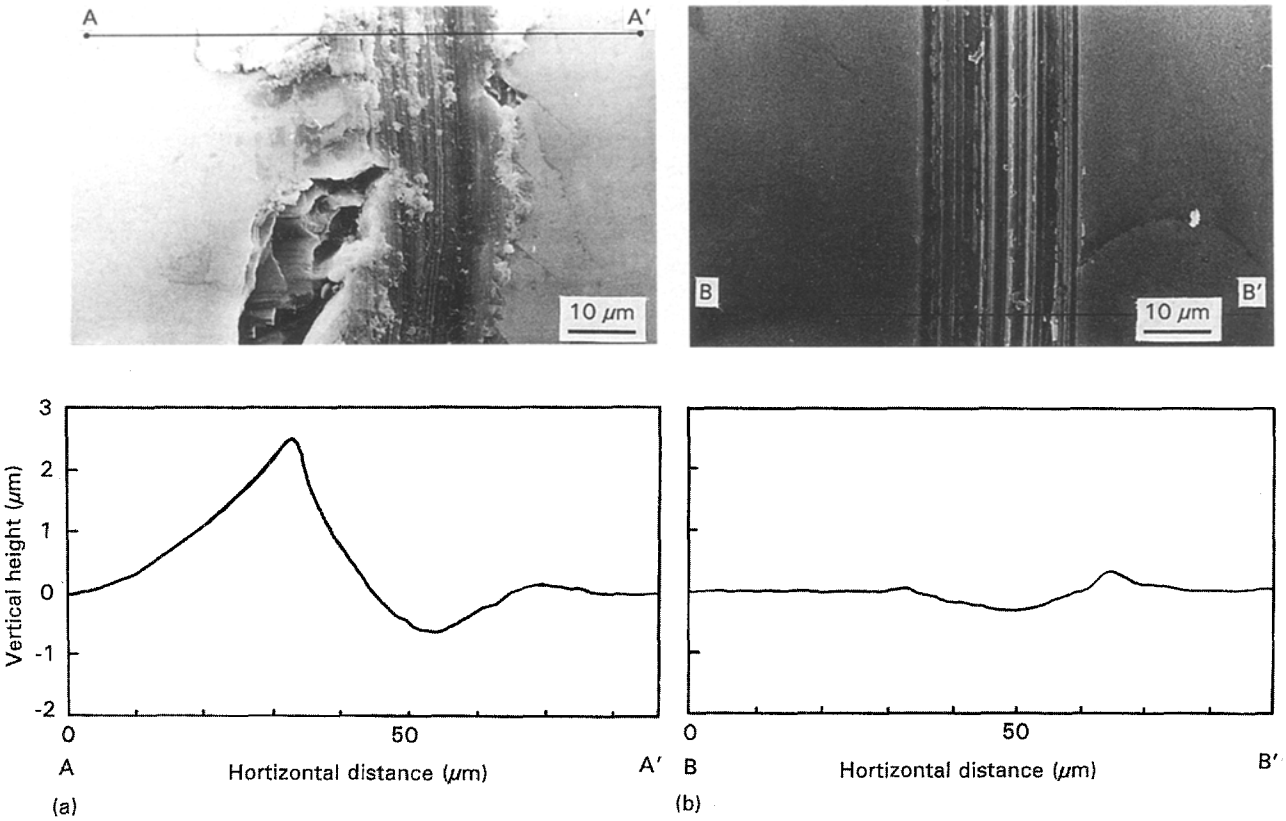

Figure 3 Secondary scanning electron micrographs and surface profilometer traces of 500 g scratches in (a) unimplanted (1 0 $\bar{1}$ 2) sapphire and (b) 5×10^{17} cm^{-2} yttrium implanted (1 0 $\bar{1}$ 2) sapphire. Subsurface lateral cracking in the unimplanted material causes the surface uplift visible in the profilometer traces. In the implanted specimen, both the radial and lateral cracking around the scratch has been reduced.

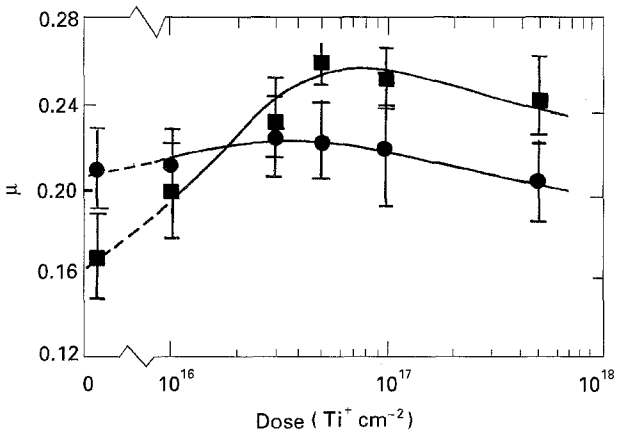

Figure 4 Variation of the coefficient of friction with dose for titanium-implanted (1 0 $\bar{1}$ 2) sapphire. The friction coefficient increases at low doses up to a maximum at the onset of amorphization. Above this dose the friction is reduced due to the presence of the soft amorphous layer. (■) 25 g, (●) 50 g.

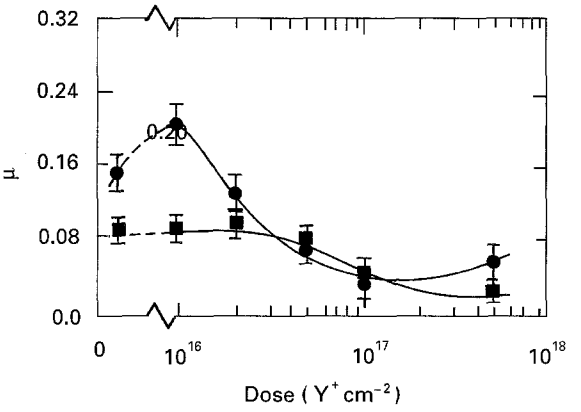

Figure 5 Variation of the coefficient of friction with dose for yttrium-implanted (1 0 $\bar{1}$ 2) sapphire. The friction increases up to a maximum at around the onset of amorphization. There is also an increase in friction at the highest doses due to the effects of ploughing through the soft amorphous layer. (■) 25 g, (●) 50 g.

the data from the 25 and 50 g traces were used; in this case, the friction force is expected to be dominated by adhesion and ploughing. Fig. 4 shows a plot of coefficient of friction against dose for titanium-implanted sapphire. The friction increases at low doses up to a maximum at the onset of amorphization, when it begins to decrease again. Above this dose, as the amorphous layer thickens, the coefficient of friction decreases until the dose at which the amorphous layer reaches the surface, when the friction has dropped below the value for unimplanted sapphire (50 g load).

TABLE III Amorphization doses for implanted sapphire

Ion	Energy (keV)	Subsurface amorphization dose, ϕ_{crit} (10^{16} ions cm^{-2})	Surface amorphization dose, ϕ_{crit} (10^{17} ions cm^{-2})
Ti	300	8.2	3.6
Y	300	2.8	1.1

Similar behaviour is observed for yttrium-implanted sapphire (Fig. 5). Table III shows the doses at which amorphization starts in the titanium- and yttrium-implanted sapphire (as determined by

Rutherford backscattering [17]) and the doses at which the amorphous layer reaches the surface (as calculated from the model of Burnett and Page [8]). The friction increases up to the dose where amorphization starts below the surface. As the amorphous layer thickens the friction is reduced until it falls to a value less than that for unimplanted material. When the amorphous layer reaches the surface the friction begins to increase again. The low-dose increase in friction is similar to the results of Burnett and Page [21].

4.2. Ploughing friction

The hardness of ion-implanted sapphire is known to increase for low-dose implantation. If the changes in friction are dominated by changes in ploughing behaviour, then the variation in friction with dose should be directly related to the variation in hardness with dose. Experimentally, the form of the friction against dose plot is found to be very similar to the form of the hardness–dose plot for the same specimens (see, for example Fig. 6). It is thus tempting to attribute the change in friction to the change in hardness of the surface layer because no cracking is observed at the loads used in this study.

The ploughing friction calculated from the Bowden and Tabor model (Equation 3 using measured values of d (Fig. 7) and P' equal to the measured hardness) may be compared to the ploughing friction calculated from the Suh model (Equation 11). Fig. 8 shows a plot of coefficient of friction against dose for yttrium-implanted sapphire scratched with a 40 μm radius diamond stylus at 25 and 50 g. Also plotted on these graphs is the ploughing friction calculated from the Bowden and Tabor model and the Goddard and Willman model as detailed by Suh. The agreement between the ploughing friction calculated by the two models is quite good for the implanted specimens. However, the agreement with the measured friction is not good. At low doses the measured friction increases whilst the calculated ploughing friction decreases. Because there is no fracture contribution, the difference can only be due to the adhesion friction mechanism. Although the hardening of the implanted layer increases P', and might be expected to increase μ_p, the

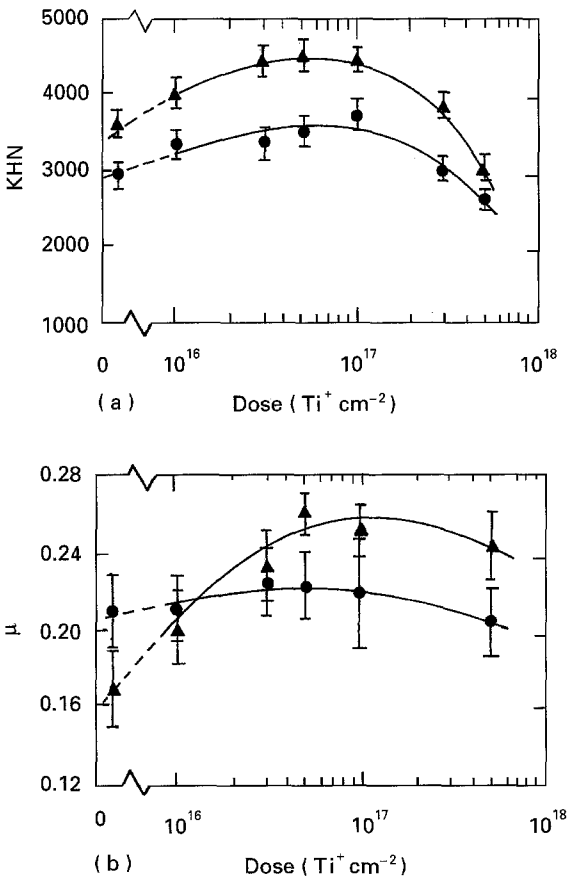

Figure 6 Comparison between the dose variation of (a) the Knoop hardness and (b) the coefficient of friction for titanium-implanted (1 0 $\bar{1}$ 2) sapphire from Fig. 4. Both show an increase up to around the dose where amorphization occurs and a decrease at higher doses. Thus it is tempting to attribute the change in friction behaviour to the change in plasticity of the surface layer produced by ion implantation. (▲) 25 g, (●) 50 g.

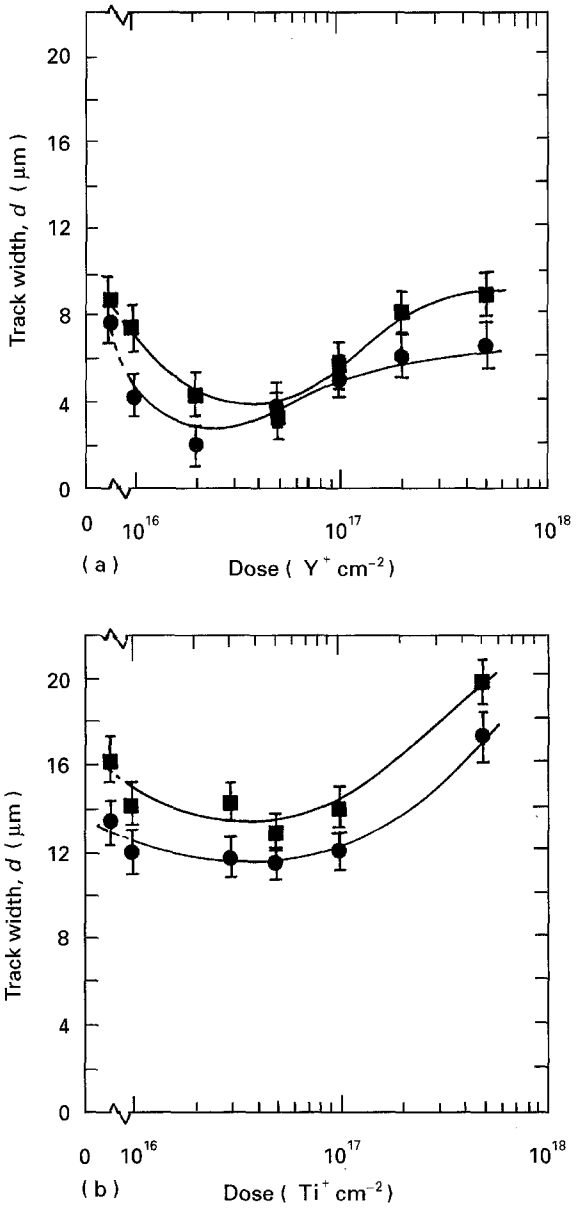

Figure 7 Dose variation of the width of scratch tracks produced by the diamond cones scratching (a) yttrium-implanted and (b) titanium-implanted (1 0 $\bar{1}$ 2) sapphire. As the hardness of the implanted surface increases, the width of the scratch track decreases. On amorphization, the surface is softened and the scratch track width increases again. (●) 25 g, (■) 50 g.

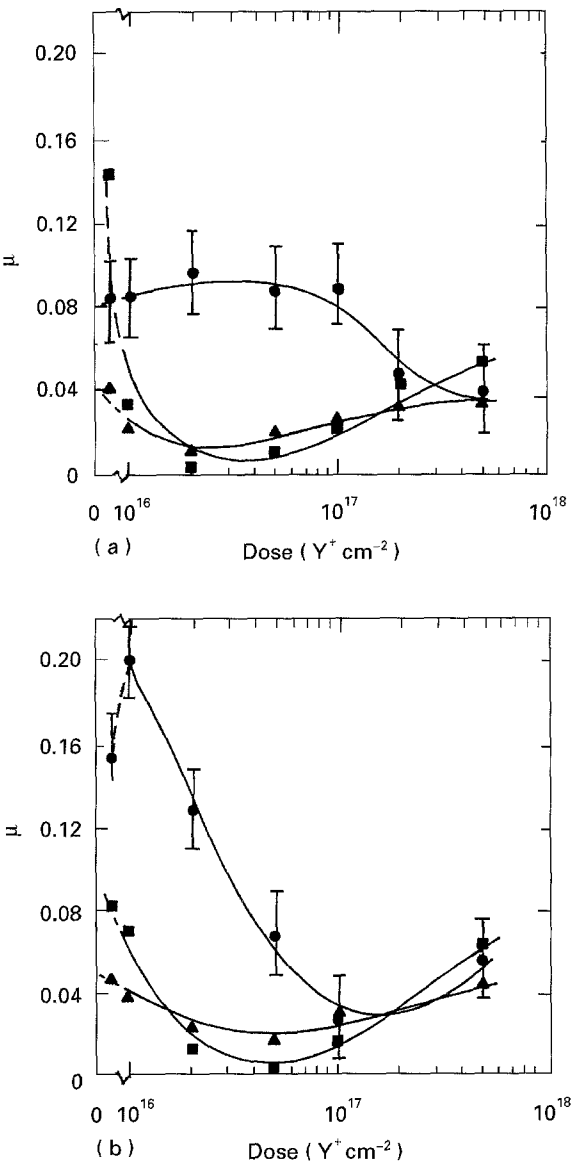

Figure 8 Variation of (●) the measured coefficient of friction, μ, with dose for yttrium-implanted (1 0 $\bar{1}$ 2) sapphire at (a) 25 g load and (b) 50 g load. Also plotted is the calculated ploughing friction according to the models of (▲) Goddard and Willman and (■) Bowden and Tabor; the error bars have been removed for clarity. Whilst the measured friction increases at low doses the ploughing friction is reduced. Thus the increase in friction at low doses must be due to changes in adhesion. At high doses, the measured friction is reduced and the ploughing friction increases until the two are nearly coincident. The friction behaviour is dominated by ploughing at these doses.

associated narrowing of the scratch track is a more significant effect and thus the ploughing friction decreases in cases where ion implantation leads to surface hardening. On amorphization the scratch width is increased again and the ploughing friction increases despite the fact that the amorphous material is softer. The measured friction is reduced until it is comparable with the ploughing friction at doses where the amorphous layer reaches the surface. Above this dose there is an increase in both the measured friction and the calculated ploughing friction, due to the fact that ploughing through the thickening amorphous layer is dominating the friction behaviour. Thus it is the width of the scratch (and hence the area of contact) that dominates the friction behaviour which depends on the hardness of the surface layer. However, the increased forces needed to plough through the harder material do not dominate the friction response.

From Fig. 8 it can be seen that for 25 g scratches the dose at which the observed friction is a maximum is $\sim 2 \times 10^{16}$ Y ions cm^{-2} and the friction does not decrease rapidly until above 10^{17} Y ions cm^{-2}. For 50 g scratches the maximum is below 10^{16} Y ions cm^{-2} and the observed friction decreases above this dose. This is due to the penetration depth of the scratch diamond. For the 25 g scratch the diamond will not penetrate into the amorphous material until a dose of 1×10^{17} Y ions cm^{-2}. For the 50 g scratch the larger penetration depth in a given specimen results in penetration into amorphous material at a dose of 5×10^{16} Y ions cm^{-2}. Thus, the rapid drop in friction is associated with the formation of amorphous material.

Fig. 9 shows the same plot for titanium-implanted sapphire. Here there is poor agreement between the Bowden and Tabor ploughing friction and the value determined from the Goddard and Willman equation. The observed friction is much higher for this material than the yttrium-implanted sapphire, whereas the calculated ploughing friction is of a similar magnitude. Thus it would appear that the effects of adhesion are more pronounced for titanium-implanted sapphire than for yttrium-implanted sapphire. It is not until 5×10^{17} Ti ions cm^{-2} that the effects of ploughing through the soft amorphous material become important.

The difference between the calculated ploughing friction curve and the experimentally determined curves at low doses is thus due to adhesion, because changes in the ploughing component cannot account for the observed trends. This is discussed in more detail in the next section.

4.3. Adhesion

From the previous section it is apparent that the increase in friction at low doses is due to a mechanism other than ploughing as was initially expected, which could be an increase in adhesion between the diamond and the substrate. In order to test this hypothesis, scratching experiments were performed with smooth spheres of relatively large radius at low loads so that no visible deformation was produced on either the sphere or the polished flat [33]. In this case the friction is expected to be dominated by adhesion.

Friction tracks were made with 1.5 mm radius spheres chosen to give a range of interfacial contact situations. Each sphere was rotated and "run-in" on unimplanted materials until they gave repeatable, consistent friction readings, between passes on the implanted materials. Five passes were made on each specimen at loads of 25 and 50 g. For these loads, no visible deformation (as observed by reflected light microscopy or SEM) occurred in the unimplanted material.

Fig. 10 shows plots of the coefficient of friction against dose for the sapphire, steel and WC/Co spheres sliding against titanium-implanted sapphire.

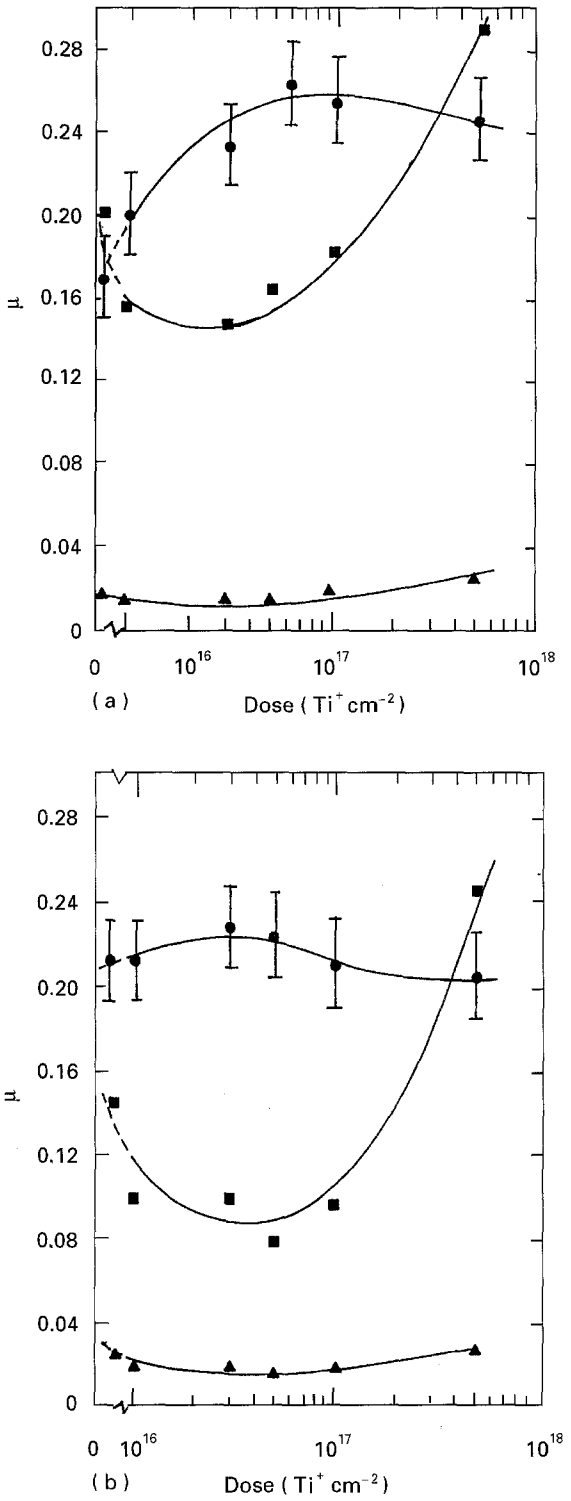

Figure 9 Variation of (●) the measured coefficient of friction, μ, with dose for titanium-implanted (1 0 $\bar{1}$ 2) sapphire at (a) 25 g load, and (b) 50 g load. Also plotted is the ploughing friction calculated using the models of (▲) Goddard and Willman and (■) Bowden and Tabor. The error bars have been removed for clarity. Again the measured friction increases whilst the calculated ploughing friction decreases at low doses, showing the importance of adhesion at these doses. At the onset of amorphization the measured friction decreases, but remains significantly larger than the increasing ploughing friction. This is due to the fact that the blunter cone used to scratch this material will have a larger surface in contact with the implanted flat and thus adhesion will be more important.

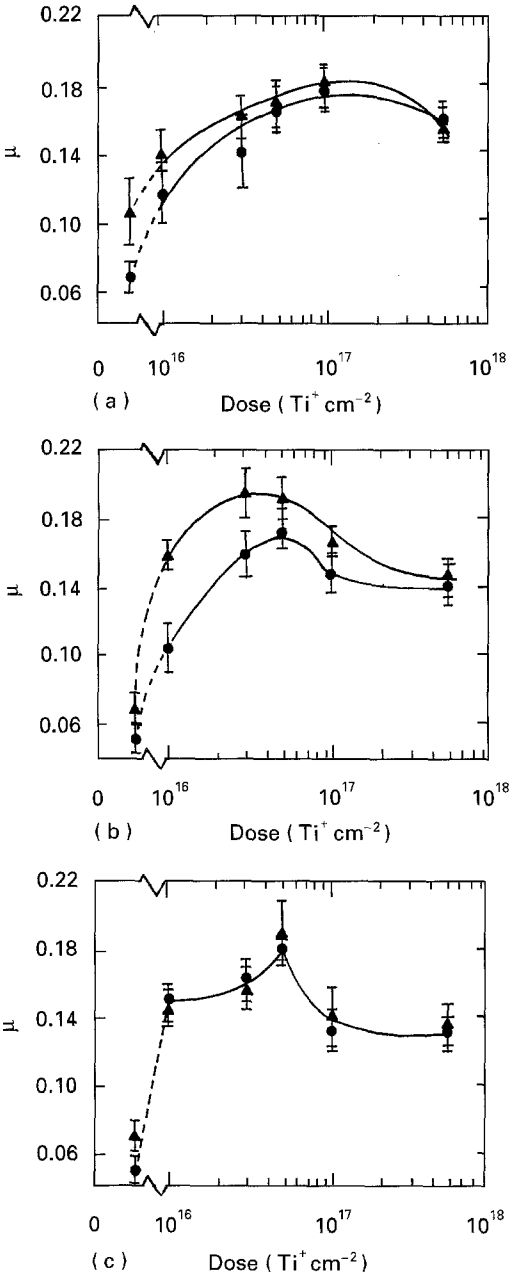

Figure 10 Variation of the coefficient of sliding friction with dose for (a) sapphire, (b) steel and (c) WC/Co spheres sliding on titanium-implanted (1 0 $\bar{1}$ 2) sapphire flats. For the sapphire sphere the friction increases up to the dose at which the amorphous layer extends to the surface, whereas for the other spheres the friction maximum occurs at the onset of subsurface amorphization. (▲) 25 g, (●) 50 g.

The behaviour is different for each of the sliders used. For the sapphire sphere (Fig. 10a) the coefficient of friction increases up to a dose of 1×10^{17} Ti ions cm^{-2} when it starts to be reduced. In the steel and the WC/Co cases the peak in friction is at a lower dose ($\sim 5 \times 10^{16}$ cm^{-2}). No sign of scratch tracks was visible on any of the flats after scratching titanium-implanted sapphire. The friction coefficients for the WC/Co sphere were found to be virtually independent of load. The dose at which the peak occurs for the sapphire sphere corresponds to the dose at which the amorphous layer reaches the surface. For the other spheres the friction peak occurs closer to the dose at which amorphization starts below the surface.

Similar friction plots for yttrium-implanted sapphire are shown in Fig. 11. For the sapphire sphere the friction increases up to a dose of 1×10^{17} Y ions cm^{-2} which is also around the dose where the amorphous layer reaches the surface. For the other spheres there were initial increases in friction at the lowest dose

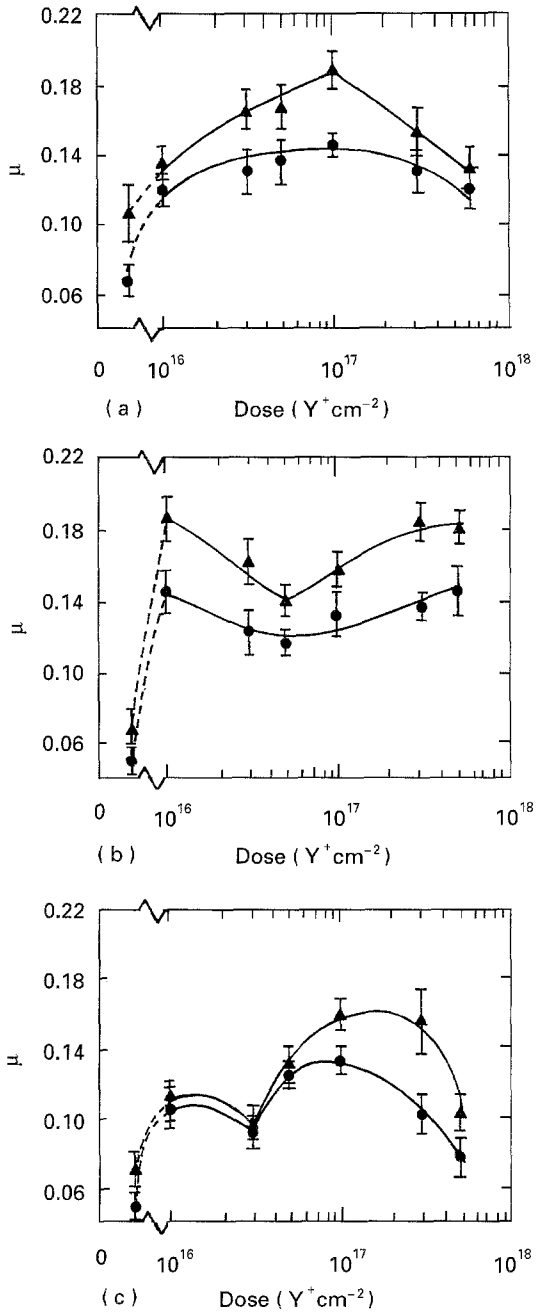

Figure 11 Variation of the coefficient of sliding friction with dose for (a) sapphire, (b) steel and (c) WC/Co spheres sliding on titanium-implanted (1 0 $\bar{1}$ 2) sapphire. For the sapphire sphere the friction increases up to the dose at which the amorphous layer extends to the surface. For the other spheres the behaviour is more complicated, though there is a friction maximum at the onset of subsurface amorphization as for the titanium-implants. (▲) 25 g, (●) 50 g.

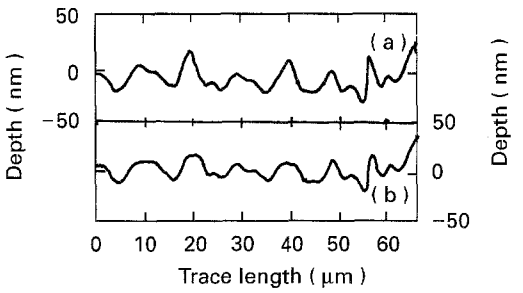

Figure 12 Surface profilometer traces along the same line on the surface of a 1×10^{17} Y ions cm^{-2} implanted (1 0 $\bar{1}$ 2) sapphire flat (a) before scratching, (b) after a single pass with a steel sphere loaded to 50 g. The asperities of the implanted surface have been flattened by the slider showing that some plastic deformation has occurred even if no visible scratch track has been produced.

(1×10^{16} Y ions cm^{-2}) but at doses above this the friction decreases until a dose of 5×10^{16} Y ions cm^{-2}. In this material the onset of amorphization below the surface is $\sim 2.8 \times 10^{16}$ Y ions cm^{-2} and thus this low-dose peak is similar to that observed for the titanium-implanted flat. At higher doses the friction increases again and visible scratch tracks are observed in the implanted flat. This increase is thus due to ploughing of the sphere through the soft amorphous material. For the WC/Co spheres there is a further decrease in friction at 5×10^{17} Y ions cm^{-2}.

The increase in friction observed for these scratches must be due predominantly to changes in adhesion between the slider and the implanted flat. However, the contact between the slider and the flat will not be uniform over the contact area, but will consist of discrete contacts at a number of asperities. For the implanted flats the polish is sufficiently good that the asperities are only 60 nm high and ~ 6 μm wide as measured by stylus profilometry. There may be some plastic deformation at the tips of these asperities, but there was no visible profilometry flattering of the asperities in surface traces across the friction tracks in any of the implanted specimens, except where well-defined scratch tracks were produced. In this case the asperities of the implanted flat were somewhat flattened. Such behaviour can be seen in surface profilometer traces along the same line before and after a scratch has been made (Fig. 12).

For true elastic contact, the frictional energy will be dissipated as heat but this will be modified by non-ideal contact situations. Dislocations may be generated at the tips of some asperities where the contact stresses are highest and thus some energy can be dissipated in plastic deformation. The presence of surface films will also contribute to the dissipation of frictional energy. Thick films may be plastically deformed, scraped from the surface and/or pushed ahead of the slider thus tending to increase the measured friction. Alternatively, the films may interfere with the slider/substrate adhesion and produce changes in the adhesion component of friction. As the thickness of such surface films is reduced, the mechanical effects of the films will become less important and changes to their adhesion to the substrate will be the major effects likely to contribute to the measured friction. Careful degreasing is expected to leave the surface with only a thin contaminant film.

Friction coefficients for ceramic materials measured in air tend to be much smaller than those measured in inert gases or under vacuum [34, 35]. This is due to the presence of adsorbed surface layers (chiefly water on oxides) which reduce the adhesion between flat and slider. Thus one possible explanation for the changes in adhesion could be the removal or disruption of these adsorbates. The presence of these adsorbates is known to produce substantial softening of the surface layer in MgO and other ceramics [36]. Bull and Page [37] have reported that ion implantation reduces this chemomechanical effect by altering the affinity of the

surface for water in some way, leading to changes in measured friction. The presence of the adsorbate will have several effects on these frictional properties; for example, they may facilitate sliding by physically separating the moving surfaces (hydrodynamic lubrication). This is likely to occur at much smaller loads than used in this study. Alternatively, the adsorbates may interfere with the adhesion of asperities (boundary lubrication). It is this mechanism which is most likely to be operating in this situation.

In the single-pass tests, such adsorbed layers may be being scraped off or pushed ahead of the slider. To see if this has a major effect on the measured friction, multiple pass tests were made on each specimen. Initially ten passes were made with the same sphere in the same direction. No changes in the measured friction coefficients were found after these tests. Similarly, reciprocating tests were performed with five passes in each direction and very good agreement was found with the friction coefficients measured for a single pass for every friction coefficient determined, regardless of sliding direction. It thus seems likely that the adsorbate layer is thin enough that it will interfere with adhesion, but not with ploughing or other friction mechanisms.

The friction of ion-implanted ceramics thus depends on the nature of the contact between the slider and the flat, together with the surface and near-surface structure of the implanted layer. For the sapphire on sapphire contact, once the amorphous material extends to the surface, the friction is reduced implying that the adhesion between amorphous material and the slider is less than that between the damaged-but-crystalline material and the slider. However, if the slider is steel or WC/Co the maximum in friction occurs when amorphization occurs below the surface. In this case some long-range effect seems to be important.

There are two potential long-range effects which could explain these observations.

1. *Subsurface plastic deformation.* In a sliding elastic Hertzian contact, the maximum shear stresses occur below the surface if the friction is low and thus this is where initial yielding is expected to occur. The depth at which this maximum occurs is about one-third the contact diameter for a spherical slider, which is well below the implanted layer. As the friction coefficient increases this maximum shear stress occurs closer to the surface, until for $\mu = 0.5$, it occurs at the surface. If the measured friction coefficient for the WC/Co and steel spheres was much higher than that for the alumina sphere the shear stresses would be larger in the subsurface amorphous layer and this could lead to yielding. However, there is no difference in the magnitude of the measured friction and so this mechanism is unlikely.

2. *Changes in elasticity.* As well as modifying the plastic properties of the surface of a material, ion implantation has been shown to reduce the elastic constants of silicon by $\sim 30\%$ once amorphization has taken place [38]. Such a change will decrease the effective elastic behaviour of the implanted substrate and increase the Hertzian contact area. If this increase in apparent contact area is mirrored by a change in real contact area the adhesion component of friction will increase even if the interfacial shear strength remains unchanged. Thus it might be expected that the friction would continue to increase after amorphization which is not observed. However, as the contact area increases the mean pressure on the contacting asperities of a real surface will be reduced. The strength of the junction between the asperities on the implanted flat and the slider will depend on the surface chemistry of each and the magnitude of this contact pressure. High pressures can generate strong bonds by squeezing and disruption of contaminant films which tend to separate the sliding surfaces. In the case of the sapphire slider on the implanted sapphire flat, such large pressures are maintained right up to the moment the amorphous layer extends to the surface. However, for the steel and WC/Co sliders there are relatively soft phases present in the near-surface microstructures of the stylus which can plastically deform to reduce the contact pressure. The chances of squeezing contamination out and forming intimate contacts between asperities on the implanted flat and these materials are thus lower and anything which reduces the contact pressure will lead to a reduction in the strength of interfacial junctions and hence the adhesion component of friction. It is for this reason that sub-surface amorphization leads to a reduction in the measured friction for these sliders.

4.4. Evidence for adhesion: material transfer

From the previous observations it can be seen that it is the nature of the contact between the slider and the flat which is important in determining the friction between the two materials. In this study three different slider materials have been used, sapphire, steel, and WC/Co, all of which are expected to have different contact properties. To understand the in-service wear properties of a material it is necessary to look at the material transport between flats and sliders after several passes. In order to investigate this, the spheres were used to make multiple passes on 5×10^{17} Y ions cm^{-2} and 5×10^{17} Ti ions cm^{-2} implanted sapphire on the hope that these high doses should enable material transfer to be detected by EDX in the SEM (though if this transfer is related to the adhesion between the slider and the flat, it should be more important at low doses). Twenty passes were performed with each sphere on the implanted flats, and the debris adhering to the spheres and left around the tracks was examined. EDX is not sensitive enough to pick up the atomic-scale material transfer over the whole contact area – Auger analysis would be better for this but the technique was beyond the scope of the present study.

In the case of titanium-implanted sapphire, debris could be found adhering to the sapphire sphere, but not to either the steel sphere or the WC/Co sphere. EDX revealed that this debris was titanium-rich and thus some bond formation between the titanium-implanted sapphire and the sapphire sphere must have occurred during the test. The debris is bound strongly enough to survive after prolonged ultrasonic cleaning

but may be removed by brushing with a soft cloth. For the yttrium-implanted flat, no debris was found to adhere to the steel sphere, though debris was found to adhere to both the WC/Co and sapphire spheres. This debris was found to be yttrium-rich by EDX in the SEM. This is similar to the titanium case and implies that the adhesion between the sphere and the implanted flat will be important in any wear mechanism that operates. For these materials the soft, plastically deformed debris adheres to the slider and flat and is not removed during the wear process. This may be important if ion-implanted ceramic components are to be used for tribological applications.

4.5. Dependence of adhesion on ploughing

Calculated shear strengths for the sapphire spheres sliding on titanium- implanted and yttrium-implanted sapphire are shown in Fig. 13. According to the model of Bowden and Tabor the shear strength increases from around 36 MPa in the unimplanted material to 93 MPa in the 1×10^{17} ion cm^{-2} implanted case for both ions (because the maximum friction is the same in both cases). A similar increase is obtained using the model of Goddard and Willman. The decrease in shear strength on amorphization is small compared to the increase before.

The increase in adhesion up to the dose at which the amorphous material reaches the surface is linear with dose for these materials. This implies that the change is dependent on the concentration of implanted atoms (or the damage they cause) in the surface region of the material. Chemical bonding between the sphere and the flat is important in the adhesion processes as well as any removal of adsorbates produced by ion implantation [33, 37]. This will depend on the precise surface chemistry produced by ion implantation.

For the scratches with the diamond indentors described in Section 4.2, the effects of adhesion on friction will be masked by the fact that considerable shear deformation of the implanted material will occur during the scratch test. In this case the interfacial shear strength must be replaced by the shear strength of the softer material (i.e. the implanted layer) and it is thus expected that μ will vary as the hardness of the implanted layer.

Using the model of Goddard and Willman (Equations 12) it is possible to calculate the shear stresses for the sapphire specimens scratched with diamond cones discussed in the previous section. In this case the adhesion friction was calculated by subtracting the calculated ploughing friction from the measured friction. From this the interfacial shear stress, τ, was calculated using Equation 12. The results are shown in Fig. 14. It is immediately obvious that the shear stresses are much larger than those calculated for the sapphire spheres. Indeed the shear stress increases closely mirror the observed hardness behaviour for these materials (see, for example, Fig. 6) for both titanium and yttrium implantation. This is further evidence that it is shear within the implanted layer which is controlling the adhesion friction properties.

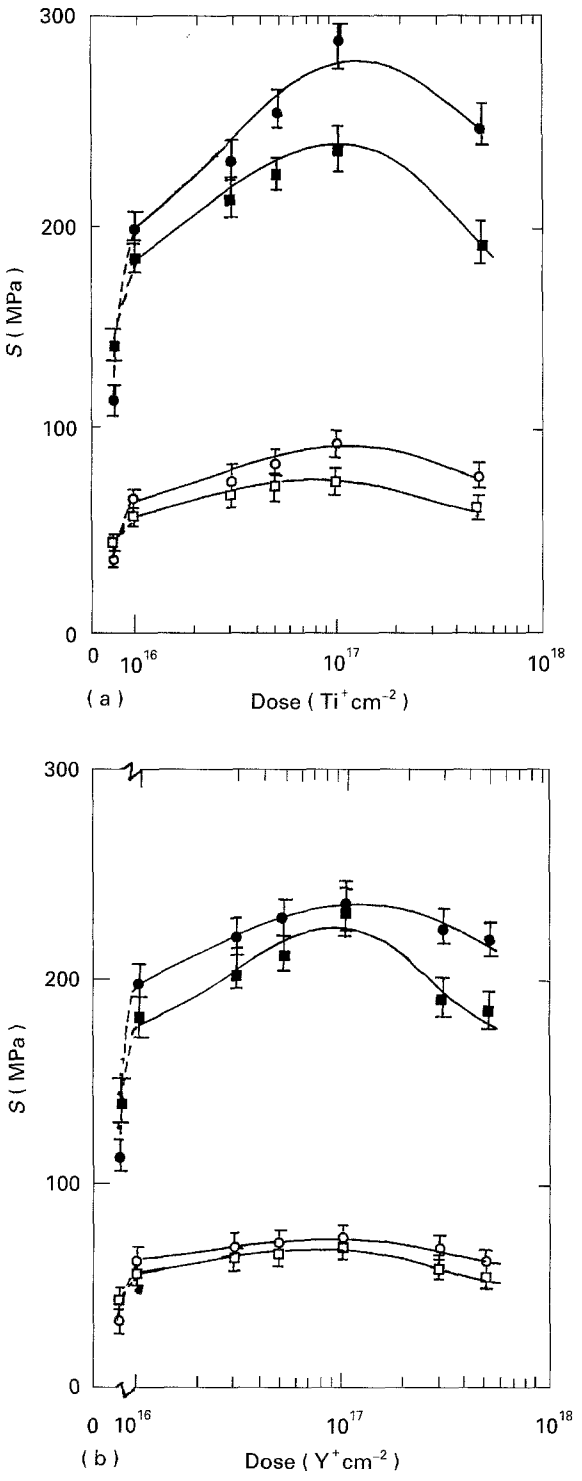

Figure 13 Dose variation of the calculated interfacial shear strengths, S, for sapphire spheres sliding on (a) titanium-implanted and (b) yttrium-implanted $(1\,0\,\bar{1}\,2)$ sapphire flats. The values were calculated according to the models of (□, ○) Bowden and Tabor and (■, ●) Goddard and Willman. Though the values calculated from the Goddard and Willman model are somewhat higher, both models predict the same trends; the shear stress increases up to the dose when the amorphous layer extends to the surface and is slightly reduced above this dose (it is still larger than for the unimplanted material). (□, ■) 25 g, (○, ●) 50 g.

For the scratch diamond, the maximum shear stresses generated by the implantation of titanium or yttrium into sapphire are different, whereas they were more comparable for the spheres. Indeed the shear strength of 2×10^{16} Y ions cm^{-2} is larger than the bulk shear stress of unimplanted sapphire (usually it is

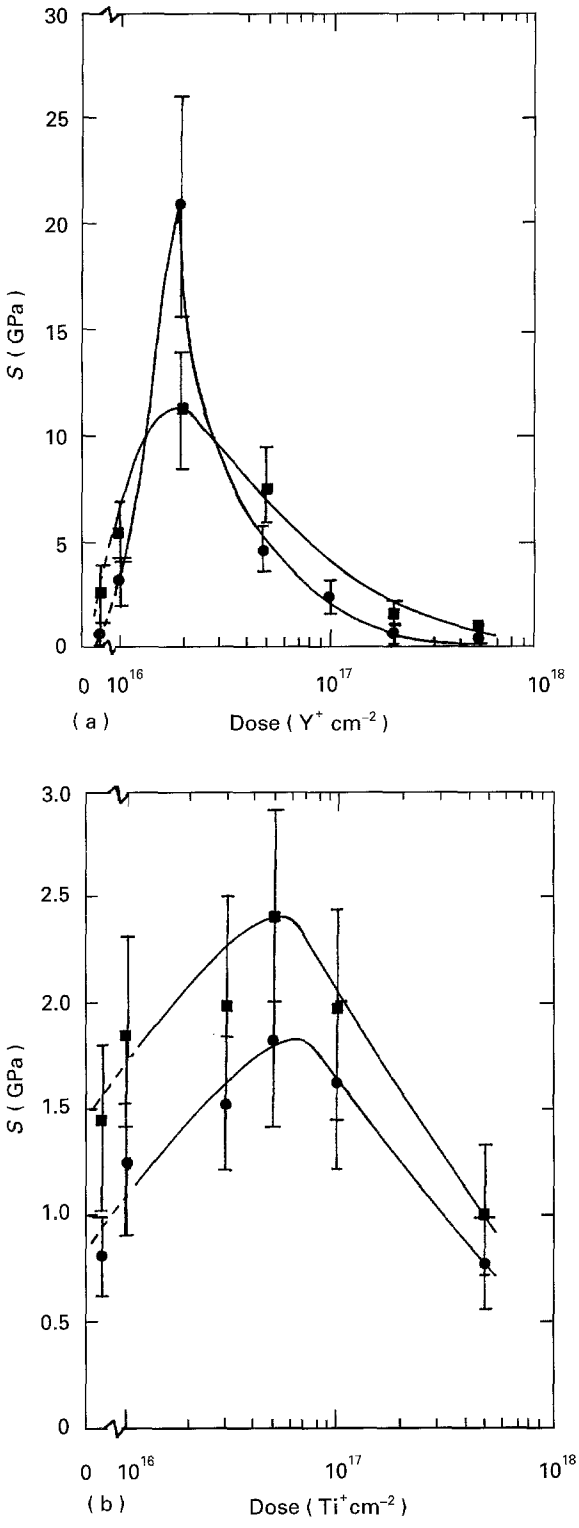

Figure 14 Variation of the interfacial shear strength with dose for (a) yttrium-implanted (1 0 $\bar{1}$ 2) sapphire, (b) titanium-implanted (1 0 $\bar{1}$ 2) sapphire scratched with a diamond cone. In this case, where plastic deformation (i.e. scratch track formation) has occurred, the interfacial shear strengths are larger than for the spheres sliding on implanted flats. The shear strength increases upto the dose at which the diamond contacts amorphous material below the surface and is then reduced. These shear strengths were calculated from the model of Goddard and Willman [30]. (●) 25 g, (■) 50 g.

assumed that for an ideal material $\tau = P/6$, see Section 3, which for a 50 g load gives $\tau = 5$ GPa). This implies that the interface is stronger than the implanted material next to it and the failure would be expected to occur in the implanted material rather than at the interface. This is known to occur for

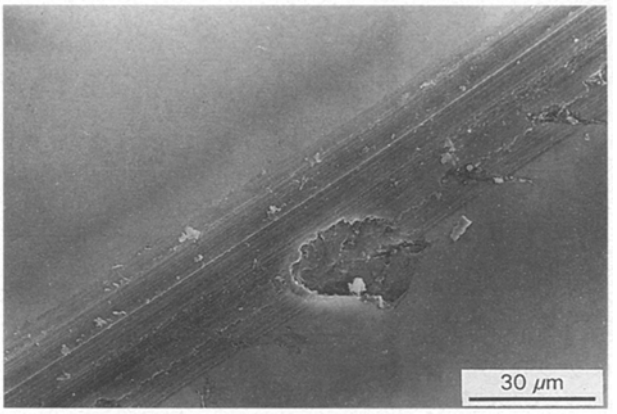

Figure 15 Secondary scanning electron micrograph (30 kV) of a 500 g scratch in 1×10^{16} Y ions cm^{-2} implanted (1 0 $\bar{1}$ 2) sapphire. A region of surface has adhered to the scratch diamond and has been pulled out of the specimen surface as the diamond passes, because the interfacial shear strength is larger than the shear strength of sapphire.

atomically clean ceramics sliding against metal pins in vacuum [39]. Fig. 15 shows a 500 g scratch track in 1×10^{16} Y ions cm^{-2} implanted sapphire. An area of material has been pulled out of the scratch track during the scratch and become adhered to the indentor. The pit left in the track does not look like the pit left when a lateral crack breaks out and a chip is formed beside the scratch. Thus it seems that the origin of this pit is in the shear failure of the implanted material, rather than by any visible fracture process. Lateral chipping is greatly reduced by ion implantation – the lateral cracks are pushed deeper and do not tend to break out – and in this specimen no evidence could be found that lateral cracking had occurred. Thus it seems that in this material a new wear mechanism can operate. Whereas sapphire normally wears by brittle fracture of plastic ploughing, some adhesive wear has occurred which will have important implications if the material is to be used for tribological applications.

It is interesting to note that the shear strength of the amorphous material is much lower than the unimplanted material. Indeed for the yttrium-implanted sapphire once the amorphous layer reaches the surface the shear strength of the surface layer drops virtually to zero. It is this low shear strength which gives the amorphized material its good lubricating properties, leading to very low friction in any contact situation. It is only when gross ploughing through the soft amorphous layer occurs at high implantation doses that the friction begins to increase again.

5. Conclusions

This paper has shown the importance of changes in indentor/substrate adhesion on the friction behaviour of ion-implanted ceramics.

For diamond cones sliding on implanted sapphire flats, the friction increases with dose until the diamond first contacts amorphous material, when it is reduced. This has been shown to be a function of shear deformation rather than ploughing. The shear strength of the amorphous material is much lower than that of a

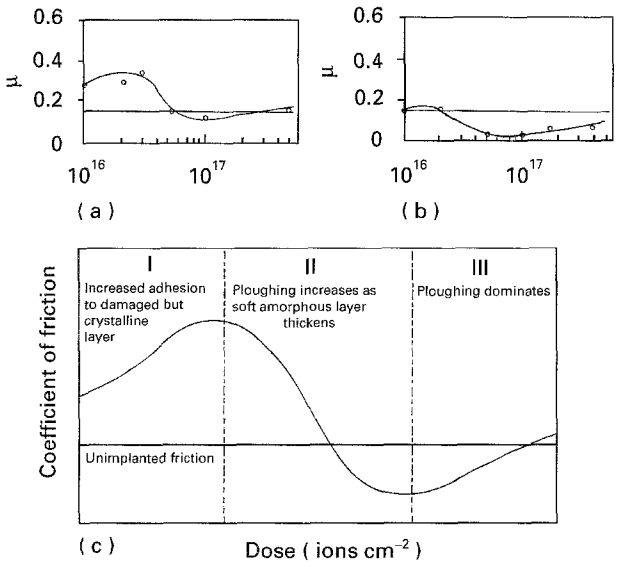

Figure 16 Variation of the coefficient of friction with dose for (a) titanium-implanted and (b) yttrium-implanted (10$\bar{1}$2) sapphire scratched with a sharp diamond cone. (●) 25 g. (c) Schematic variation of the coefficient of friction with dose. The friction initially increases due to the increasing adhesion between the slider and the implanted flat (Region I). At the onset of subsurface amorphization the friction is reduced as this adhesion is reduced and the effects of ploughing through the soft amorphous layer become important (Region II). At the highest doses, ploughing behaviour dominates and the thickening surface amorphous layer results in a slight increase in friction (Region III).

crystalline material. At the very highest doses the friction increases again with dose, due to the effects of ploughing through a thickening soft surface layer. This behaviour is shown schematically in Fig. 16.

For a range of sphere materials sliding on implanted sapphire flats, similar increases in friction were determined with dose. However, in this case, where the ploughing component of friction is small, the friction increases up to the dose where amorphization occurs below the surface, or where the amorphous layers reach the surface, depending on the nature of the contact between the materials. This difference in behaviour has been attributed to differences in asperity deformation between the contacting materials.

From these results a number of conclusions may be drawn.

1. Ion implantation changes the friction and wear behaviour of ceramics. The changes depend on the choice of ion, energy and dose together with the ceramic and slider material.

2. Low-dose ion implantation increases the hardness of alumina and this leads to a reduction in ploughing friction and abrasive wear.

3. The ploughing friction depends on the cross-sectional area of the scratch track and flow stress of the material. Whereas increasing hardness will increase the flow stress and hence increase ploughing friction, the reduction in the area of the scratch track for the harder material will more than counteract this and the ploughing friction is reduced as the ceramic surface is hardened by ion implantation.

4. At high doses, ion implantation leads to amorphization of alumina and other ceramics leading to surface softening and reduced abrasion resistance.

5. At very high doses, the increase in scratch track area in the softened amorphous material will greatly outweigh any reductions in flow stress. For this reason the ploughing friction increases as surface softening occurs.

6. Accompanying the increase in hardness at low implantation doses is an increase in the adhesion between stylus and the implanted layer. This manifests itself as an increase in measured friction.

7. The increased friction due to adhesion disappears on amorphization. For some slider materials, this happens at the onset of amorphisation below the surface, whereas for others, it occurs when the amorphous layer extends to the surface.

8. Ion implantation leads to increase in adhesion by the disruption of surface adsorbates [37].

9. If implanted components are to be used for tribological applications, the presence of the implantation-induced stresses will reduce the wear due to fracture. The hardened surface layer will also reduce the plastic abrasive wear at doses below the onset of amorphization. However, the increase in adhesion/shear strength at these doses may result in the increase of adhesive wear and such a change in wear mechanism could affect the use of ion-implanted components.

Acknowledgements

The authors thank colleagues at Harwell and the Universities of Cambridge and Newcastle for useful discussions.

References

1. D. H. BUCKLEY, "Surface effects in friction, wear and lubrication" (Elsevier, Amsterdam, 1981).
2. F. P. BOWDEN and D. TABOR, "The friction and lubrication of solids Part I," (Clarendon Press, Oxford, 1958).
3. E. RABINOWICZ, "Friction and wear of materials" (Wiley, New York, 1965).
4. N. P. SUH, "Tribophysics" (Prentice-Hall, Englewood Cliffs, NJ, 1986).
5. G. DEARNALEY, *Thin Solid Films* **107** (1983) 315.
6. I. SINGER, *Mater. Res. Soc. Symp. Proc.* **27** (1984) 585.
7. S. G. ROBERTS and T. F. PAGE, in "Ion implantation into metals," edited by V. Ashworth, W. A. Grant and R. P. M. Proctor (Pergamon, Oxford, 1982) pp. 135.
8. P. J. BURNETT and T. F. PAGE, *J. Mater. Sci.* **19** (1984) 845.
9. *Idem, ibid.* **19** (1984) 3524.
10. *Idem, Rad. Eff.* **97** (1986) 123.
11. C. J. McHARGUE, *Int. Met. Rev.* **31** (1986) 49.
12. H. NARAMOTO, C. W. WHITE, J. M. WILLIAMS, C. J. McHARGUE, O. W. HOLLAND, M. M. ABRAHAM and B. R. APPLETON, *J. Appl. Phys.* **54** (1983) 683.
13. J. K. COCHRAN, L. O. LEGG and H. F. SOLNICK-LEGG, *Mater. Res. Soc. Symp. Proc.* **24** (1984) 173.
14. T. HIOKI, A. ITOH, S. NODA, H. DOI, J. KAWAMOTO and O. KAMIGAITO, *J. Mater. Sci.* **21** (1986) 1321.
15. C. S. YUST and C. J. McHARGUE, *Mater. Res. Soc. Symp. Proc.* **17** (1982) 533.
16. C. J. McHARGUE, G. M. BEGUN, J. M. WILLIAMS, C. W. WHITE, B. R. APPLETON, P. S. SKLAD and P. ANGELINI, *Nucl. Instrum. Meth.* **B16** (1986) 212.
17. S. J. BULL and T. F. PAGE, *J. Mater. Sci.* **23** (1988) 4217.
18. N. E. W. HARTLEY, *Wear* **34** (1975) 427.
19. *Idem, Thin Solid Films* **64** (1979) 177.

20. *Idem*, *Mater. Res. Soc. Symp. Proc.* **7** (1982) 295.
21. P. J. BURNETT and T. F. PAGE, *Wear* **114** (1987) 85.
22. N. P. SUH and H. C. SIN, *ibid.* **69** (1981) 91.
23. M. V. SWAIN, *Proc. R. Soc. Lond.* **A366** (1979) 575.
24. B. R. LAWN and M. V. SWAIN, *J. Mater. Sci.* **10** (1975) 113.
25. B. R. LAWN and R. WILSHAW, *ibid.* **10** (1975) 1049.
26. B. R. LAWN and A. L. EVANS, *ibid.* **12** (1977) 2195.
27. G. R. ANSTIS, P. CHANTIKUL, B. R. LAWN and D. B. MARSHALL, *J. Am. Ceram. Soc.* **64** (1981) 533.
28. J. M. CHALLEN and P. L. B. OXLEY, *Wear* **53** (1979) 229.
29. C. A. BROOKES, *Philos Mag.* **A43** (1981) 529.
30. J. GODDARD and H. WILLMAN, *Wear* **5** (1965) 114.
31. D. M. MARSH, *Proc. Roy. Soc.*, **A279** (1964) 420.
32. R. HILL, "Theory of plasticity" (Oxford University Press, Oxford, 1950).
33. S. J. BULL and T. F. PAGE, *Nucl. Instrum Meth.* **B32** (1988) 91.
34. D. H. BUCKLEY, in "Surfaces and interfaces in glass and ceramics, materials science research 7", edited by V. D. Frechette, W. C. La Course and V. L. Burdick (Plenum Press, New York, 1974) pp. 101–26.
35. T. E. FISCHER and H. TOMIZAWA, *Wear* **105** (1985) 29.
36. A. R. C. WESTWOOD, J. S. AHEARN and J. J. MILLS, *Coll. Surf.* **2** (1981) 1.
37. S. J. BULL and T. F. PAGE, *J. Phys. D Appl. Phys.* **22** (1989) 941.
38. P. J. BURNETT and G. A. D. BRIGGS, *J. Mater. Sci.* **21** (1986) 1828.
39. D. H. BUCKLEY, *Mater. Res. Soc. Symp. Proc.* **40** (1985) 359.

Received 10 March
and accepted 5 April 1995